RSC Advances

PAPER

View Article Online
View Journal | View Issue

Cite this: *RSC Adv.*, 2023, **13**, 11182

Hydroxy silicone oil modified boron nitride for high thermal conductivity and low dielectric loss silicone rubber composites: experimental and molecular simulation studies†

Xiao Yu,[a] Bo Qiao,[b] Fei Cai,[c] Ji-hai Xiao,[a] Wei Yang*[b] and Si-zhu Wu *[a]

Polymer-based composites are widely used in microelectronics and wireless communications, which require high thermal conductivity and low dielectric loss for effective heat dispersion and signal transmission. Different lengths of hydroxyl silicone oil chains modified boron nitride/silicone rubber composites were explored and prepared in this work. Experiments demonstrate that the long-chain modified BN improves the thermal conductivity and decreases the dielectric loss of composites. A molecular dynamics simulation was employed to study the mechanism and affecting variables. The calculated results indicated that the improvement of the thermal and dielectric properties is mainly related to the interfacial behavior, including interfacial compatibility, interfacial bond strength, and phonon matching. Based on the simulated interfacial behavior and thermal conductivity, the thermal and dielectric properties of different chain-length modified boron nitride/silicone rubber composites have been anticipated. The results show that the longer-chain modified boron nitride/silicone rubber composites have better thermal and dielectric properties. This research may give a theoretical foundation for the development of materials with designable performance for electronic devices.

Received 20th January 2023
Accepted 2nd April 2023

DOI: 10.1039/d3ra00428g

rsc.li/rsc-advances

1. Introduction

Due to the fast advancement of information technology and the downsizing, low weight, and high integration of electronic devices, it is essential to manage the operating temperature to maintain the stability and service life of electronic equipment. Therefore, the problem of heat dissipation in materials has become a formidable obstacle.[1–4] Materials with large dielectric losses in tiny communication devices cause signal dissipation to rise and produce more heat, which is unfavorable for use in these scenarios.[5–8] Heat management materials require excellent thermal conductivity, suitable dielectric characteristics, and good insulating qualities.

Conventional polymer-based materials are widely used in thermal management materials due to their excellent processing properties, low dielectric loss, and good electrical insulation performances.[9] Among them, silicone rubber, with its excellent flexibility, is commonly used in electronic packaging because of its remarkable resistance to radiation in a wide range of applications at different temperatures and humidity levels.[10] However, the poor thermal performance of silicone rubber, with a thermal conductivity of only 0.2 W m^{-1} K^{-1}, greatly limits its application.[11–13] Thus, the development of silicone rubber composites with excellent thermal conductivity becomes a priority.

To solve this problem, high thermal conductivity fillers like silver (Ag),[14] graphene (GE),[15] carbon nanotubes (CNT),[16] alumina (Al_2O_3),[17] and boron nitride (BN)[18] are often added to rubber composites. Among them, metal and carbon materials present better electrical conductivity with wide applications. However, in applications that need electrical insulation, such as electronic packaging, thermal interface materials, *etc.*, the usage of these fillers may be limited.[19] Boron nitride is of interest in ceramic materials due to its high thermal conductivity with low dielectric loss and strong breakdown strength, which has a high usage value.[20] Liu *et al.* added boron nitride to silicone rubber to improve the breakdown strength and thermal conductivity of the composites, although the dielectric loss increased with higher BN loading.[21] Poor dispersion is usually the main problem with inorganic fillers/polymer composites. It is reported that weak interfacial interactions and strong interfacial polarization are mostly to blame.[22] Furthermore, the interface between the BN sheet and the polymer matrix has a high interfacial thermal resistance. This has the potential to reduce the effectiveness of thermal conductivity enhancement.[23]

[a]*State Key Laboratory of Organic–Inorganic Composites, Beijing University of Chemical Technology, Beijing 100029, China*

[b]*Beijing Institute of Smart Energy, Beijing 102209, China. Email: 19630100@163.com*

[c]*Shenzhen Geim Graphene Center (SGC), Tsinghua-Berkeley Shenzhen Institute (TBSI), Tsinghua Shenzhen International Graduate School (TSIGS), Tsinghua University, Shenzhen 51805, China*

† Electronic supplementary information (ESI) available. See DOI: https://doi.org/10.1039/d3ra00428g

In order to improve the interfacial properties, researchers usually functionalize BN.[24] Fillers covalently modified with organic molecules have been found to be beneficial in modulating the dielectric and thermal properties of BN/polymer composites. Yang *et al.* added boron nitride coated with polydopamine modified with silane coupling agent to a natural rubber matrix filled with 30 vol% boron nitride composites, the thermal conductivity was increased to 0.26 W m^{-1} K^{-1} and the dielectric loss was only 0.25 at 10^2 Hz.[23] Jiang *et al.* grafted poly(glycidyl methacrylate) links on the BN surface and added 15 vol% of modified boron nitride to the epoxy resin. The thermal conductivity was improved by 505% over the pure epoxy resin, and the dielectric loss tangent was about 0.065 at 10^4 Hz.[25] However, most of the above works have focused on experimental aspects, and the quantitative understanding of the mechanism is still insufficient. Moreover, it is difficult to distinguish the effects of multiple factors by experimental tests due to the complicated conditions.[26]

In recent years, molecular dynamics (MD) simulations have become an important and easy-to-use tool for studying the micromechanics of materials.[27] Wu *et al.* used MD simulations to investigate the relationship between the number and size of hexagonal boron nitride nanosheet (h-BN) layers and the thermal conductivity of h-BN/paraffin composites. It was found that to obtain composites with high thermal conductivity, the number of layers and lateral dimensions of h-BN must be increased simultaneously.[28] Ma *et al.* studied the mechanism of the effect of three functionalizations, *i.e.*, C-doping, $-CH_3$ grafting, and single vacancies, on the thermal conductivity of boron nitride nanosheet (BNNS)/paraffin composites by MD simulations. The functionalization was found to promote the in-plane and out-of-plane phonon coupling of BNNS, thus promoting the energy propagation between paraffin and BNNS and ultimately increasing the interfacial thermal conductivity.[29] However, there are fewer studies on the effect of grafted organic chain length on the thermal and dielectric properties of boron nitride/silicone rubber composites, and most of the studies on the mechanism have focused on phonon coupling, with less exploration of the interfacial mechanism, especially in a quantitative way.

In this research, different chain lengths of hydroxy silicone oil, with a similar molecular structure to that of silicone rubber chain, were used as the modifier to graft on BN. It was designed and utilized with the expectation of improving the interfacial properties of the composites. In addition, it is hoped that through a combination of experiments and molecular simulations, the effects of grafted chain length on the composite properties can be investigated. The microscopic mechanisms of the changes in thermal conductivity and dielectric properties of BN composites modified with different chain lengths may be analyzed at the molecular level to provide a theoretical basis for the modification and regulation of the composite interfaces.

2. Experimental section

2.1 Materials

BN (size ~10 μm) is produced by Dandong Chemical Research Institute. High-hydroxyl-value hydroxyl silicone oil (hydroxyl value 8.18%, kinematic viscosity 30 mm^2 s^{-1}) and low-hydroxyl-value hydroxyl silicone oil (hydroxyl value 3.91%, kinematic viscosity 45 mm^2 s^{-1}) are purchased from North New Sihai Chemical Co. Dibutyltin dilaurate was obtained from Shanghai Aladdin Co. Xylene and anhydrous ethanol are produced by Beijing Chemical Factory. Silicone rubber 112-0 (SiR, MW of 6×10^5 g mol^{-1}) was purchased from Dongjue Organosilicon Co. All the materials were industrial grade and used as received without further treatments.

2.2 Methods

2.2.1 Preparation of hydroxy silicone oil modified BN. The boron nitride powder was placed in a muffle furnace and annealed at 1000 °C for 2 h. The annealed BN was washed three times with deionized water to produce hydroxyl-modified boron nitride (BNO). Take 1 g of BNO dispersed in 100 ml of xylene solution, add hydroxy silicone oil (HSO, 10 g) to the suspension, and add 0.01 g of dibutyltin dilaurate, and react at 100 °C for 8 h. The resulting solution was washed by filtration through a microporous filter membrane (50 mm in diameter, pore size 0.22 μm). The product was washed with ethanol and water to remove xylene and impurities. After 7 h at 60 °C and 3 h at 140 °C in a vacuum oven, two kinds of boron nitride modified by hydroxy silicone oil with different chain lengths were obtained.

2.2.2 Preparation of composite materials. The BN, or modified BN, DCP, and SiR were mixed on a double-roller open plastic refiner (Shanghai Rubber Machinery No. 1 Factory, China). As the boron nitride content increased from 10 wt% to 40 wt%, the mixing time of the blends was increased from 10 min to 50 min to ensure the uniform dispersion of the boron nitride particles in the matrix. Then the compounds were vulcanized at 160 °C for an optimal time, which was determined by a disc rheometer (Beijing Ruida Yuchen Instrument, China).

2.3 Characterization

For the Fourier transform infrared (FT-IR) measurements, a Bruker Tensor 27 spectrometer (Bruker Corporation, Germany) in transmission mode was employed. Using a TGA/DSC3+ (Mettler, Sweden) with a heating rate of 10 °C min^{-1} in a nitrogen environment, thermogravimetric analysis (TGA) was conducted. On an Escalab 250 XPS system, X-ray photoelectron spectroscopy (XPS) was conducted utilizing an Al K radiation source (Thermo Electron Corporation, USA). Wide-angle X-ray diffraction (WXRD) studies were conducted on Cu K radiation ($\lambda = 1.541$) to use a WXRD-6000 diffractometer (Shimadzu Corporation, Japan). Water contact angle testing was performed through a droplet shape analyzer (Kruss, Germany). The fracture surfaces of the specimens were observed by scanning electron microscopy (SEM) (Hitachi, Japan) using a Hitachi S-4800 system. The isotropic thermal conductivity of the samples (sample thickness ~6 mm) was measured by a TPS1500 hot disk thermal conductivity meter (Hot disk, Sweden). An Alpha-A broadband dielectric spectrometer (Novocontrol, Montabaur, Germany) was used to test the dielectric characteristics in the frequency range of 10^{-1} to 10^6 Hz at 220 V at ambient temperature. The dielectric breakdown characteristics

were investigated using a high-voltage DC generator (DTZH-60, Multi-Tech Electric, China) operated at a ramp rate of 1 kV s^{-1} until electrical breakdown occurred.

3. Simulation section

3.1 Model details

In this study, molecular chains of silicone rubber with the number of repeating units of 50 were constructed using dimethylsiloxane as repeating units.[30] Two hydroxy silicone oils with different chain lengths were modeled by calculating a number of repeating units from the hydroxyl values. Their number of repeating units provided from the manufacturer was set to 5 and 11, and the corresponding hydroxy silicone oils were named HSO5 and HSO11, respectively. In order to predict the thermal and interfacial properties of BN grafted with longer chain length silicone oil chains, a longer chain length silicone oil chain model containing 20 repeating units (with the name of HSO20) was also constructed, and the size of the BN model was about 26.889 Å × 25.489 Å. In addition, modified boron nitride models of Si5, Si11, and Si20 were constructed by grafting these three silicone oils onto BN. The simulation models of hydroxy silicone oil, silicone rubber, the constructed equilibrium kinetics, and heat transfer are shown in Fig. 1. The process of constructing the equilibrium kinetic model for calculating the interface properties and the laminar model for thermal conductivity calculations is shown in ESI 2.† The atomic level contacts at the interface after equilibrium are shown in Fig. S2.†

3.2 Equilibrium molecular dynamics simulation

Molecular dynamics (MD) simulations were performed using the Forcite module in Materials Studio software (Accelrys, USA), and the Dreiding force field was chosen to describe the molecular interaction.[31] To calculate the interfacial properties of the composite systems, an amorphous model of the BN filler/SiR system with five SiR chains in each cell was constructed for calculating the solubility parameter (δ), binding energy ($E_{binding}$), free volume fraction (FFV), and mean square displacement (MSD). The intelligent algorithm was used for energy minimization in the amorphous cells.[32] Afterwards, the cells were annealed once again between 300 and 500 K for 100 cycles, with 10 heat gradients per cycle. Then, the amorphous cells were subjected to an NVT ensemble (constant atomic number, volume, and temperature) for 500 ps and an NPT ensemble (constant atomic number, pressure, and temperature) for 500 ps at a pressure of 1 × 10^{-4} GPa. To regulate pressure and temperature, respectively, a Berendsen air pressure regulator and an Andersen thermostat were used. The Ewald technique was used to calculate electrostatic interactions with an accuracy of 1 × 10^{-3} kcal mol^{-1}, and the Lennard-Jones function was used to calculate van der Waals interactions with a cut-off distance of 12.5 Å.[32] Additionally, all models included periodic boundaries in three dimensions.

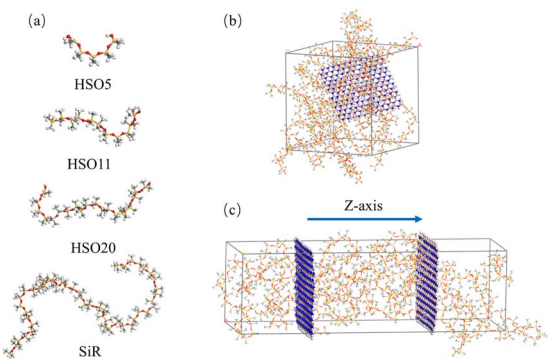

Fig. 1 (a) Three hydroxy silicone oils as well as silicone rubber (SiR) chains (b) BN/SiR system in equilibrium kinetic model (c) heat transfer model for the BN/SiR system. (Gray, white, red, and yellow spheres represent the C, H, O, and Si atoms, respectively. The unsaturated edges of BN and modified BN sheets were terminated by adding hydrogen atoms.)

3.3 Non-equilibrium molecular dynamics simulation

To calculate the thermal conductivity of the composite systems, a laminar model containing eight SiR molecular chains, as shown in Fig. 1(c), was constructed based on non-equilibrium molecular dynamics (NEMD) simulations of the Müller-Plathe method.[33,34] The thermal model must first be pre-equilibrated using the same procedure as for the equilibrium amorphous cell before determining the filler/SiR thermal conductivity. Following this, the model was separated into 100 layers along the *z*-axis. The 1st and 100th layers were customized as the hot layers, and the middle 50th layer was set as the cold layer. The energy was exchanged between the hot and cold layers in a nonphysical way.[35] The equilibrium temperature gradient along the *z*-axis was formed by calculating 500 ps under the NVE ensemble (constant atomic number, volume, and energy).

4. Results and discussion

4.1 Characterization of hydroxy silicone oil modified boron nitride

The FT-IR curves of BN and various hydroxy silicone oil modified BN (named Si5 and Si11) are shown in Fig. 2(a). The black BN curve shows the characteristic peaks at 1375 and 807 cm^{-1} that can be attributed to in-plane B–N stretching vibrations and out-of-plane B–N bending vibrations, respectively. The Si5 and Si11 curves (*i.e.*, red and blue curves) show new peaks of Si–O–Si, Si–C, and C–H stretching vibrations at 1100, 1262, and 2960 cm^{-1}, respectively. It proves that the modification of hydroxy silicone oil on BN is successful.

Fig. 2(b) shows the TGA images of BN and the Si5 and Si11. From the figure, it can be obtained that the thermal weight loss of Si5 and Si11 increased by 1.28 wt% and 4.68 wt% compared to BN. And most of the weight loss starts at over 200 °C, indicating the covalent nature of the grafted part and excluding the presence of residual solvent.

The XPS results of BN and modified BN are shown in Fig. 2(c) and Table 1, from which it can be deduced that the elemental ratios of C, O, and Si elements on Si5 and Si11 increased with the increase of the grafted silicone oil chain. The elemental

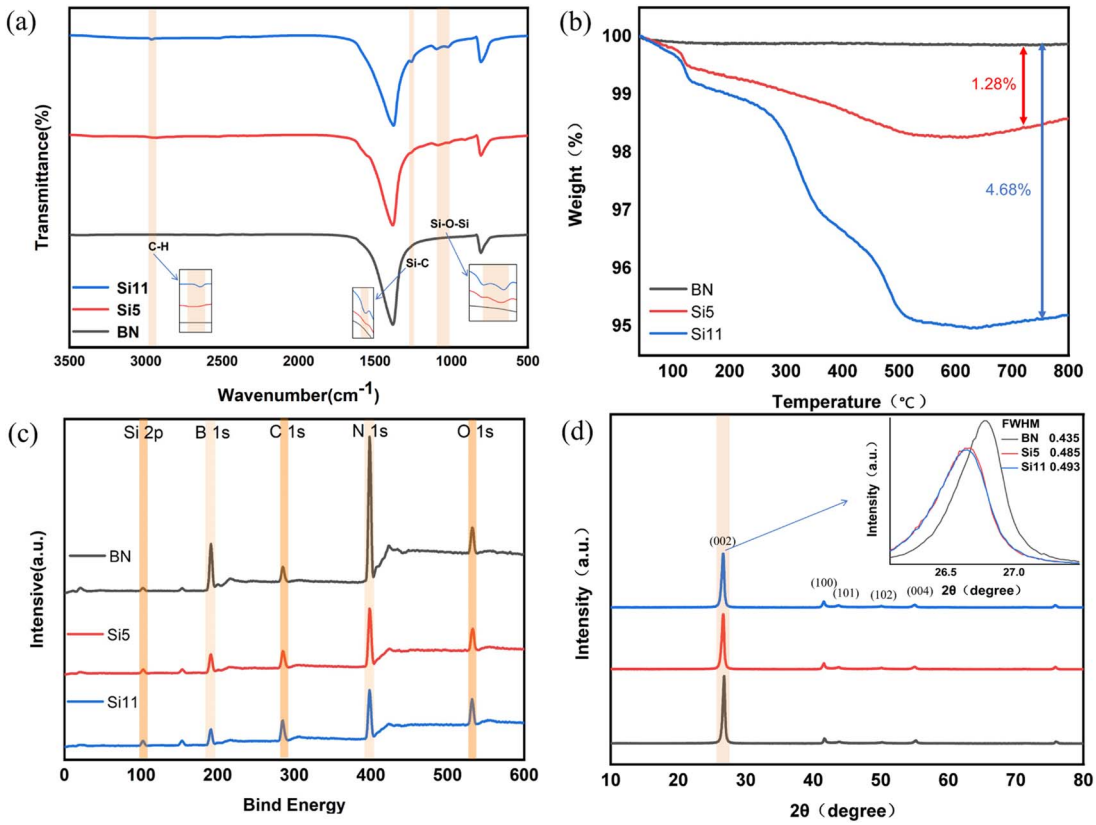

Fig. 2 (a) FT-IR, (b) TGA, (c) XPS, (d) XRD curves of BN, Si5, and Si11.

contents of C, O, and Si in Si11 increased by 11.94%, 5.13%, and 4.32%, respectively, compared to the pure BN. It is also obvious from the elemental content in Table 1 that the modification of boron nitride by hydroxy silicone oil is successful.

Fig. 2(d) shows the XRD patterns of BN, Si5, and Si11 samples. The X-ray diffraction peaks of BN at 2θ are 26.78°, 41.65°, 43.87°, 50.16°, and 55.04°, which correspond to the (002), (100), (101), (102), and (004) lattice planes of BN, respectively. Meanwhile, the full width at half maximum (FWHM) of modified BN increases at the (002) peak position, indicating that the microcrystalline size of modified BN may gradually decrease during the thermal exfoliation process. In addition, the positions of the (002) peaks of Si5 and Si11 were shifted to small angular positions of 0.13° and 0.14°, respectively, compared to BN. This indicates that the crystal plane spacing also becomes larger compared to pure BN.[36] This further indicates that BN was successfully thermally stripped and modified.

To determine the hydrophobicity effect of hydroxy silicone oil modification on BN, the water contact angles of both BN and modified BN were tested. As shown in Fig. 3, the water contact angles of Si5 and Si11 were grown at 107% and 197%, respectively, gradually changing from hydrophilic to hydrophobic. This indicates that the water contact angle of BN gradually increases with the hydroxyl silicone oil grafted on BN and that its hydrophobicity is getting better, which also means that it has better compatibility with the hydrophobic silicone rubber matrix.

Table 1 The element content of BN, Si5, and Si11 samples

Symbol	C (atom%)	O (atom%)	Si (atom%)
BN	8.12	5.22	1.84
Si5	17.6	8.74	4.23
Si11	22.06	10.35	6.16

4.2 Dispersibility of BN in silicone rubber composites

The dispersion state of the different fillers in SiR composites was observed by the SEM method, and the results are shown in Fig. 4. The presence of large BN agglomerates in the BN/SiR composites indicates that the dispersion of pure BN in the SiR matrix (Fig. 4(a)) is poor and BN cannot better form a filler network, which is not conducive to the improvement of thermal conductivity. Fig. 4(b) shows that the dispersion of BN in Si5/SiR is well improved, and no larger agglomerates can be observed in the image. However, in the enlarged Fig. 4(e), a small number of smaller agglomerates can still be seen. This is mainly due to the improved interfacial compatibility between Si5 and SiR after the hydroxyl silicone oil modified BN. It makes its dispersion in the rubber matrix better, which is beneficial for improving thermal conductivity. Fig. 4(c) and (f) present that the Si11/SiR composites have the best dispersion, with almost no agglomerates visible, indicating the optimal dispersion of Si11 in the SiR matrix, which is very beneficial for the thermal conductivity enhancement.

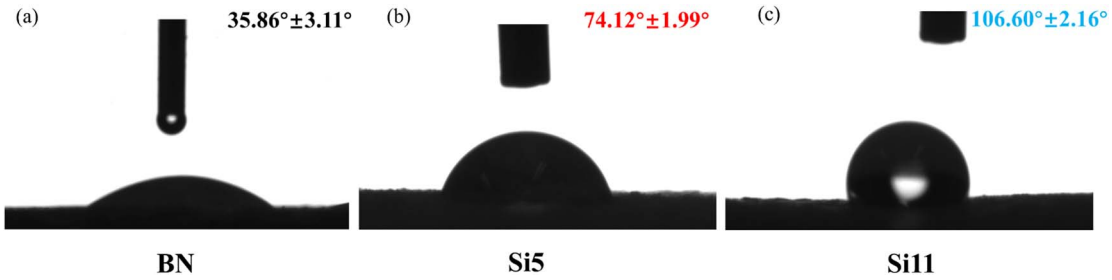

Fig. 3 Water contact angle images of (a) BN, (b) Si5, and (c) Si11.

4.3 Dielectric properties

Fig. 5(a) and (b) show the performance of the composites in terms of dielectric loss and dielectric constant, respectively. Fig. 5(a) exhibits the reduced dielectric loss of both modified BN (*i.e.*, Si5, Si11)/SiR composites compared to the pure BN/SiR. The highest values of dielectric loss of Si5/SiR and Si11/SiR are reduced by 41.8% and 74.5%, respectively, compared to BN/SiR composites. It indicates that the dielectric loss of the composites decreases as the chain length of grafted silicone oil on BN increases, and the enhancement of dielectric loss is mainly in the range of 10^{-3}–10^{2} Hz. This is in accordance with the reported literature, which states that interfacial polarization occurs mainly in the low frequency band below 10^{2} Hz, which will affect its dielectric performances.[37] Therefore, the reduced dielectric loss of BN/SiR composites with longer graft chain length may be due to the stronger interfacial interaction between the long-chain modified BN and silicone rubber, which limits the interfacial polarization and leads to the reduced dielectric loss. Fig. 5(b) shows the dielectric constants of the composites, and the performance trend is similar to the dielectric loss in Fig. 5(a). When compared to pure BN, the dielectric constants of Si5 and Si11 also went down, getting closer to the dielectric constants of pure SiR (the orange curve).

Fig. 5(c) shows the dielectric breakdown strength of the composites with different filler contents. As shown in the figure, among the samples studied, Si11/SiR exhibited the best breakdown resistance. The highest breakdown strength of Si11/SiR reaches 117.73 kV mm^{-1} when the filler content is 40 wt%, which is a 73.2% improvement compared to pure silicone rubber. The excellent breakdown strength of Si11/SiR can be explained as follows: to begin with, the inherent high breakdown strength of BN inhibits electron avalanches.[38] Secondly, the excellent interfacial forces and interfacial properties of Si11 and SiR may improve the defects present at the interface to increase the dielectric breakdown strength of the composites. On the other hand, the long-chain modified BN filler presents better dispersion in the SiR matrix compared to the pure BN, creating a denser barrier in the SiR to limit the electron tree.[38]

4.4 Thermal conductivity of composites

The thermal management properties were examined through the preparation of SiR-based composites with a series of filler loadings. The experimental values of isotropic thermal conductivity (TC) are shown in Fig. 6(a), and it is obvious that the isotropic thermal conductivity of all three composites gradually increases as the BN loading in SiR becomes larger. In

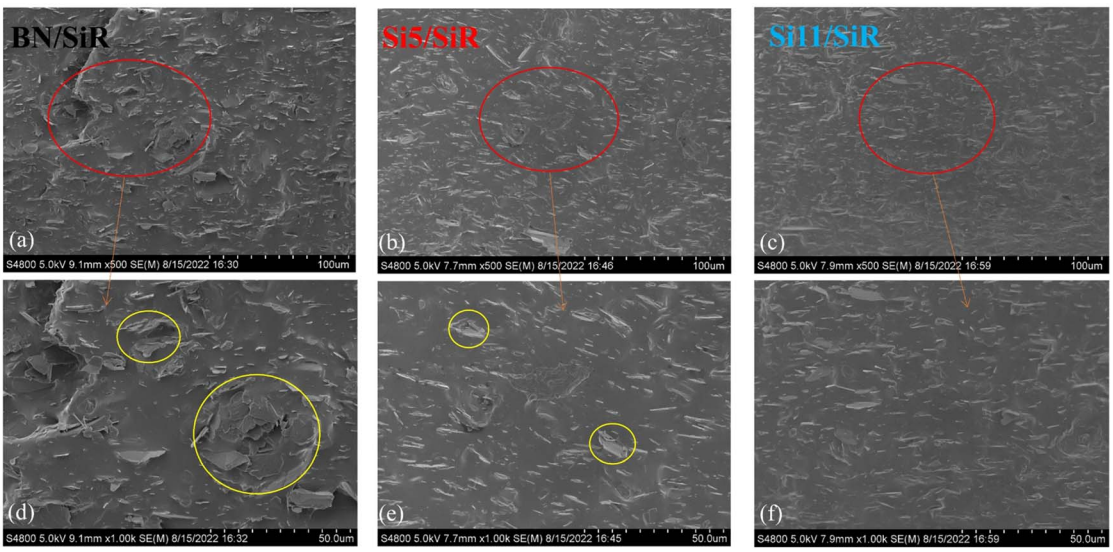

Fig. 4 Cross-sectional SEM images of (a) BN/SiR, (b) Si5/SiR, (c) Si11/SiR composites, and (d), (e), and (f) corresponding local enlargements.

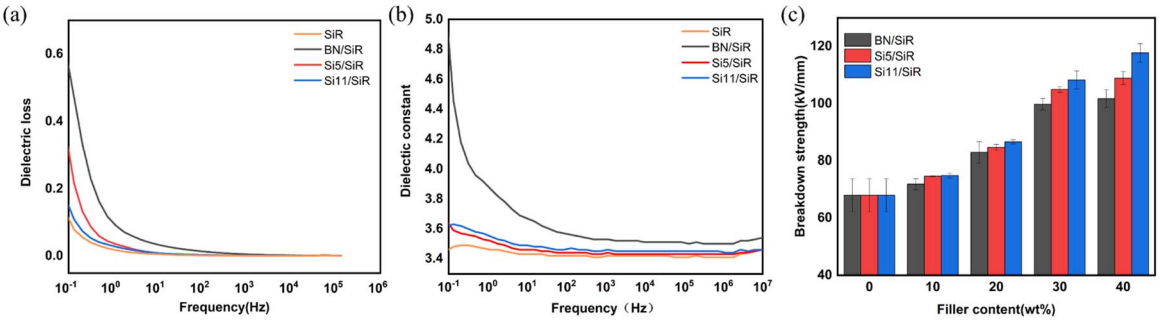

Fig. 5 (a) Dielectric loss, (b) dielectric constant, and (c) dielectric breakdown strength of pure SiR and SiR composites.

addition, the longer the chain length of grafted hydroxyl silicone oil on BN, the larger the TC value of the composites. Among them, the TC of the composites reached 1.88 W m^{-1} K^{-1} at 40 wt% Si11 in silicone rubber, which is 683.3% higher than that of pure SiR. Fig. 6(b) summarizes the previously reported data on the thermal conductivity of filled BN composites.[4,10,39–52] The data show that the long-chain hydroxy silicone oil modified BN (Si11) exhibits excellent ability in improving the thermal conductivity of the SiR composites. This illustrates what a big advantage well-designed long-chain modified BN may have in stopping phonon scattering and making the properties of the interfaces better.

In order to further verify the thermal conductivity of the composites, the infrared thermography method was attempted. In this study, four samples were placed on a heated table at a constant temperature, and their temperature changes with time were recorded with an infrared camera. From the IR thermography image in Fig. 6(c) and the thermography temperature variation in Fig. 6(d), it is found that the heating rate of the composites increases with the growth of the grafted silicone oil chain, for instance in Si11/SiR composites, which is consistent with the trend of thermal conductivity.

This further confirms that modified BN/SiR composites have better thermal conductivity. The following sections will be

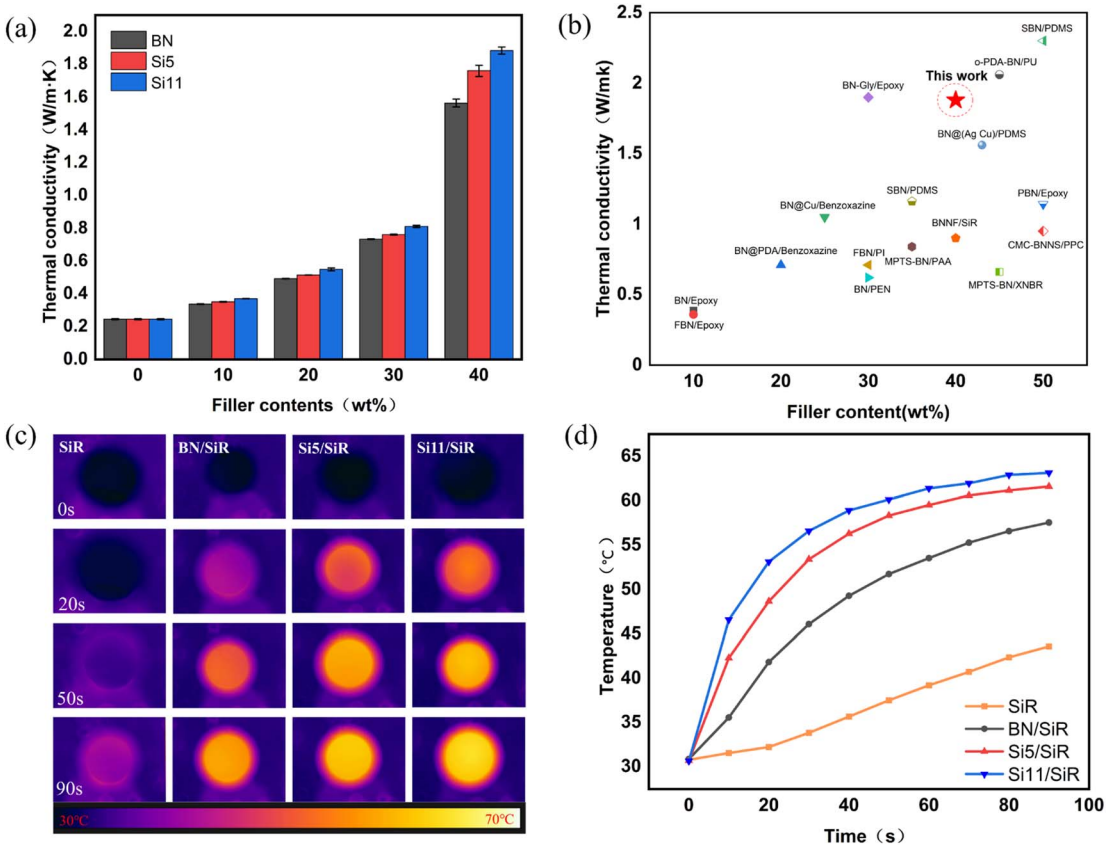

Fig. 6 (a) TC value plot for pure SiR and SiR composites, (b) statistical results of thermal conductivity of BN-based composites reported in the literature, (c) IR thermography image, (d) IR thermography temperature variation curve with time.

explored by using molecular simulations in order to further investigate and explain the mechanism of improving TC as well as dielectric properties from a microscopic perspective, as well as to uncover the effect of the chain length on the modified BN on the thermal and dielectric properties.

4.5 Compatibility analysis of fillers and substrates

According to the principle of similar compatibility, the less the gap between the solubility parameters of the filler and the matrix, in accordance with the principle of similar compatibility, the greater the thermodynamic compatibility.[53] According to the following equation, the solubility parameter δ may be derived from the square root of the cohesive energy density (CED).[54]

$$\delta = \sqrt{\mathrm{CED}} = \sqrt{\frac{E_\mathrm{V}}{V_\mathrm{m}}} \quad (1)$$

where E_V is the molar energy of vaporization and V_m is the molar volume. Table 2 lists the calculated δ values of BN, hydroxy silicone oil modified BN (Si5, Si11), and SiR. Due to the synthesis conditions, only Si5 and Si11 samples were obtained for the modified BN, but from a simulation point of view, it was desired to explore the role of longer modification chains. Therefore, we constructed a Si20 model for further prediction. It is found that the solubility parameter of BN decreases gradually as the length of grafted silicone oil chains on BN increases and gets closer to the solubility of SiR. This indicates that BN grafted with long-chain hydroxyl silicone oil contributes more to the better compatibility between the filler and the matrix. The excellent compatibility between the filler and matrix results in the uniform dispersion of BN in silicone rubber, which is advantageous for the formation of the filler network, the improvement of interface defects, and the augmentation of thermal conductivity and dielectric breakdown strength. The results show that Si20 has the lowest solubility parameter, with a decrease of 30.28% of δ compared to BN. This indicates that BN modified with the suitable long-chain hydroxy silicone oil is more beneficial to improve the interfacial compatibility of the composites.

4.6 Interfacial characterization of filler and substrate

Binding energy E_binding is defined as the negative value of the interaction energy of the two components, which can reflect the interaction of the two components through MD simulations.[55]

Table 2 Solubility parameters δ of silicone rubber (SiR), BN, and modified BN (Si5, Si11, Si20), and their differences $\Delta\delta$

	δ (J cm^{-3})$^{0.5}$	$\Delta\delta$ (J cm^{-3})$^{0.5}$
SiR	14.91 ± 0.10	—
BN	24.50 ± 0.11	9.59
Si5	22.96 ± 0.23	8.05
Si11	19.74 ± 0.19	4.83
Si20	17.08 ± 0.32	2.16

In general, the stronger the E_binding, the stronger the filler–matrix interfacial interaction:[56]

$$E_\mathrm{binding} = -E_\mathrm{inter} = -(E_\mathrm{total} - E_\mathrm{BN} - E_\mathrm{SiR}) \quad (2)$$

where E_inter, E_total, E_BN, and E_SiR are the energies of two-component interactions, the total energy of composites, and the energies of BN and SiR, respectively. Fig. 7(a) depicts the E_binding values of the pure BN/SiR and three modified systems, from which it is shown that the interfacial interaction between the modified BN and SiR matrix becomes stronger as the length of grafted silicone oil chains on the BN increases from Si5 to Si20. And the calculated binding energy of Si20 reached a high of 916.05 kcal mol^{-1}, suggesting that the strongest interfacial interaction force exists between the Si20 with the longest chain modification and the SiR matrix.

Previous study discovered that the larger the filler–matrix interfacial interaction, the tighter the stacking of its polymer chains, and the lower the FFV. The FFV is calculated as follows:[57]

$$\mathrm{FFV} = \frac{V - V^*}{V} \quad (3)$$

where V is the total volume and V^* is the occupied volume. In Fig. 7(b), it is indicated that the FFV of the grafted hydroxyl silicone oil on BN gradually becomes smaller as the chain length of the grafted silicone oil on BN increases. Therefore, it can also be seen from the FFV that the growth of grafted silicone oil chains on BN is beneficial to enhance the interfacial interaction force of the composite system. In addition, it has been discovered that the lower the FFV value, the smaller the porosity of the composite system, which aids in heat transmission.[22]

The mean square displacement (MSD) is the characteristic value of the movement of polymer chains. The stronger the interfacial interaction between the filler and the matrix, the more serious the obstruction of the movement of the polymer chain, corresponding with the smaller the MSD values. The MSD can be calculated as follows:[40]

$$\mathrm{MSD} = \langle |r_i(0) - r_i(t)|^2 \rangle \quad (4)$$

where $r_i(0)$ and $r_i(t)$ represent the positions of particle i at the initial and t moments, respectively. $|r_i(0) - r_i(t)|$ represents the displacement of atom i at moment t, and $\langle\ \rangle$ denotes the average value of the average displacement taken for all selected atoms. The order of MSD values (BN > Si5 > Si11> Si20) is shown in Fig. 7(c). This reflects that the long-chain modification (*i.e.*, Si20) corresponds to higher E_binding values and the lowest MSD values. To better quantitatively characterize the molecular chain motility, the diffusion coefficients (D) of the four systems were also calculated by MD simulations as follows:[58]

$$D = \lim_{t\to\infty}\frac{1}{6t}|r_i(0) - r_i(t)|^2 = \frac{\mathrm{MSD}}{6t} = \frac{s}{6} \quad (5)$$

where s is the slope of the mean square displacement curve for the BN/SiR system and t represents the time of particle motion. The magnitude of the D value in Fig. 7(d) indicates more intuitively that the molecular chain motility is most severely

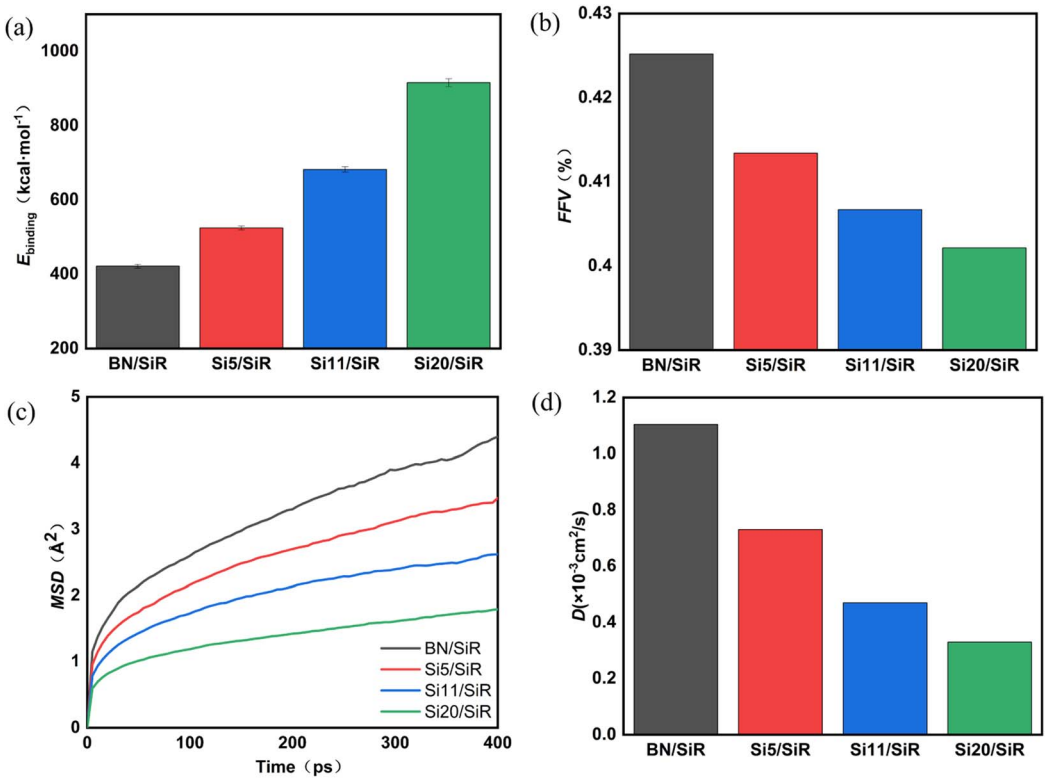

Fig. 7 (a) $E_{binding}$ diagram, (b) FFV diagram, (c) MSD curve, and (d) D diagram for different composites systems.

restricted in the Si20/SiR system, which means that the Si20 may present the strongest interfacial force.

The increase of the interfacial force makes the bond between filler and matrix tighter, hence limiting the interfacial polarization of the composites under an alternating electric field and aiding in the reduction of dielectric loss. Accordingly, this work predicts that modification will reduce the dielectric loss. In addition, stronger interfacial interactions suppress the scattering of phonons during interfacial propagation, which contributes to higher thermal conductivity, as discussed in the following.

Heat transfer in polymer matrix composites relies mainly on phonon vibrations. The fillers in the composites tend to have a low phonon vibration match with the matrix and are prone to scattering during the interfacial transport, leading to an increase in the interfacial thermal resistance. This work calculated Phonon vibration power spectrum (PVPS) values using MD simulations to further investigate how better interfacial characteristics affect phonon propagation in composites. The formula for the phonon vibration power spectrum is shown in eqn (6).[59]

$$D(\omega) = \int_0^{\tau} [\langle v(0) \cdot v(t) \rangle \cdot \cos(\omega t)] \mathrm{d}t \quad (6)$$

where $D(\omega)$ is the PVPS at a frequency of ω, $\langle v(0) \cdot v(t) \rangle$ is the velocity autocorrelation of the atom, and $v(0)$ and $v(t)$ are the velocities of the atom at times 0 and t, respectively.

The findings are displayed in Fig. 8(a). The figure demonstrates the main vibration intervals between 900–1300 cm^{-1}, 1500–2000 cm^{-1}, and 2800–3300 cm^{-1} for SiR matrices with different fillers. To further quantify the matching of phonon vibrations, this research introduces the matching coefficient (M) between the filler and the substrate, which can be calculated using the following equation:[59]

$$M = \frac{\int_0^{\infty} \mathrm{PVPS}_{\mathrm{filler}}(f) \cdot \mathrm{PVPS}_{\mathrm{matrix}}(f) \mathrm{d}f}{\int_0^{\infty} \mathrm{PVPS}_{\mathrm{filler}}(f) \mathrm{d}f \cdot \mathrm{PVPS}_{\mathrm{matrix}}(f) \mathrm{d}f} \quad (7)$$

Among them, $\mathrm{PVPS}_{\mathrm{filler}}$ and $\mathrm{PVPS}_{\mathrm{matrix}}$ denote the PVPS of the matrix and filler in the composites, respectively. In general, the better the phonon matching, the stronger the interfacial bonding, the lower the interfacial thermal resistance, and the bigger the TC, the better the thermal conductivity of the composites system.[60] It can be visualized from Fig. 8(b) that as the graft hydroxy silicone oil chain length grows (*i.e.*, from Si5 to Si20), the matching coefficient M of the composites system gradually increases, and the phonon coupling between BN and SiR at the interface improves correspondingly, which is beneficial to the thermal conductivity of the composites.

From the above calculation results, it can be seen that the long-chain hydroxyl silicone oil modified boron nitride shows better interfacial compatibility and interfacial interaction force with the silicone rubber matrix. The improved interfacial compatibility of the composites allow for better dispersion of the filler in the matrix. In addition, this is beneficial for the construction of the thermal conductivity network of the filler. The enhancement of the interfacial interaction force can reduce

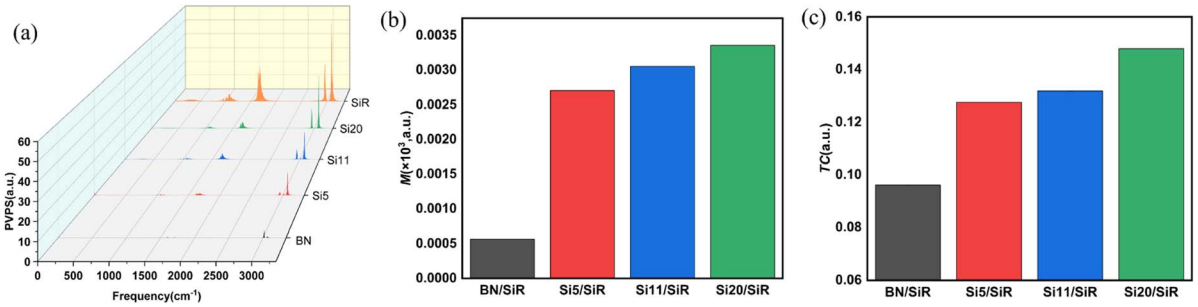

Fig. 8 (a) Phonon vibration power spectrum curves, (b) phonon matching factor *M*, and (c) simulated TC values for different composites systems.

the distance of interfacial gap, suppress phonon scattering, reduce the interfacial thermal resistance, and increase the heat transfer efficiency at the interface.[61] In addition, a strong interfacial interaction force will suppress the interfacial polarization of the composite system and reduce the dielectric loss of the composite system. In summary, BN modified with long-chain silicone oil is more beneficial to enhance the thermal and dielectric properties of the composites.

4.7 Prediction of thermal conductivity of composite systems

The NEMD approach was used to calculate the thermal conductivity values of four composite systems, and the results are displayed in Fig. 8(c).[62] The TC values of Si5, Si11, and Si20 are larger than those of the pure BN/SiR system. And the TC of the composites system becomes larger as the chain length of hydroxy silicone oil grafted on BN increases. The sequence of TC values of Si11/SiR > Si5/SiR > BN/SiR is consistent with the trend of experimental results in Fig. 6(a), (c) and (d). In addition, the theoretical TC value of Si20/SiR presents the highest simulated prediction. This suggests that a longer-chain modified Si20/SiR system may have better thermal conductivity, mainly due to the better interfacial characteristics, which improve the propagation of phonons at the interface and contribute to the improvement of thermal conductivity.

5. Conclusions

In this work, boron nitride (BN) was modified by hydroxyl silicone oil with varying chain lengths, and matching silicone rubber (SiR) composites were prepared. Combining simulation and experimentation, the dielectric and thermal characteristics of BN/SiR composites were studied. The key conclusions are as follows:

(1) As the chain length of grafted hydroxyl silicone oil on BN becomes longer, the thermal conductivity and breakdown strength of the Si5/SiR and Si11/SiR composites gradually increase, and the dielectric loss decreases. The thermal conductivity of the 40 wt% Si11 in the SiR composites increased by 683.3%, and the dielectric breakdown strength was enhanced by 73.2% compared with that of pure SiR. Its dielectric loss maximum decreased by 74.5% compared to BN/SiR. The fabricated composites demonstrated outstanding thermal and dielectric properties.

(2) The thermal conductivity trends of Si5/SiR and Si11/SiR composites are well explained by molecular dynamic simulations. As the chain length of grafted silicone oil on BN increases, its solubility parameters δ, FFV, and MSD decrease, and the binding energy $E_{binding}$, coupling factor M are enhanced, the interfacial interaction force and the interfacial compatibility of the composite system are gradually enhanced. Based on the above calculated parameters, it is predicted that the longer chain modified BN, such as Si20, is more beneficial to the thermal conductivity and dielectric properties of the composites.

In conclusion, it is envisaged that this research will give quantitative tools and a theoretical foundation for the rational design of interfacial structures of rubber composites necessary for electronic devices.

Conflicts of interest

There are no conflicts to declare.

Acknowledgements

The authors gratefully acknowledge financial support from the National Natural Science Foundation of China (Grant No. 51873017).

Notes and references

1 N. Burger, A. Laachachi, M. Ferriol, M. Lutz, V. Toniazzo and D. Ruch, *Prog. Polym. Sci.*, 2016, **61**, 1–28.
2 H. Y. Chen, V. V. Ginzburg, J. Yang, Y. F. Yang, W. Liu, Y. Huang, L. B. Du and B. Chen, *Prog. Polym. Sci.*, 2016, **59**, 41–85.
3 J. Dong, L. Cao, Y. Li, Z. Q. Wu and C. Q. Teng, *Compos. Sci. Technol.*, 2020, **196**, 108242.
4 W. Wang, M. Zhao, D. Y. Jiang, X. Zhou and J. Q. He, *Ceram. Int.*, 2022, **48**, 2763–2770.
5 D. Y. Liu, L. Y. Wu, K. Wu, S. M. Xu, G. P. Sui, M. F. Jing, J. Zhao, Y. Wei and Q. Fu, *Composites, Part A*, 2019, **119**, 134–144.
6 S. Takahashi, Y. Imai, A. Kan, Y. Hotta and H. Ogawa, *J. Alloys Compd.*, 2014, **615**, 141–145.
7 X. W. Xu, R. C. Hu, M. Y. Chen, J. F. Dong, B. Xiao, Q. Wang and H. Wang, *Chem. Eng. J.*, 2020, **397**, 125447.

8 J. Yuan, S. Yao and P. Poulin, *Polymer Nanocomposites: Electrical and Thermal Properties*, ed. X. Huang and C. Zhi, Springer International Publishing, Cham, 2016, pp. 3–28, DOI: 10.1007/978-3-319-28238-1_1.
9 Y. Xue, X. Li, H. Wang, F. Zhao, D. Zhang and Y. Chen, *Mater. Des.*, 2019, **165**, 107580.
10 B. Zhong, J. Zou, L. An, C. Ji, X. Huang, W. Liu, Y. Yu, H. Wang, G. Wen, K. Zhao and X. Lin, *Composites, Part A*, 2019, **127**, 105629.
11 X. Y. Huang, P. K. Jiang and T. Tanaka, *Ieee Electr Insul M*, 2011, vol. 27, pp. 8–16.
12 A. Li, C. Zhang and Y. F. Zhang, *Polymers*, 2017, **9**, 437.
13 Z. H. Yin, J. H. Guo and X. H. Jiang, *Compos. Sci. Technol.*, 2021, **209**, 108794.
14 Y. M. Yao, X. L. Zeng, R. Sun, J. B. Xu and C. P. Wong, *ACS Appl. Mater. Interfaces*, 2016, **8**, 15645–15653.
15 Q. R. Yang, Z. L. Zhang, X. F. Gong, E. R. Yao, T. Liu, Y. Zhang and H. S. Zou, *Heat Mass Transfer*, 2020, **56**, 1931–1945.
16 T. Kashiwagi, E. Grulke, J. Hilding, K. Groth, R. Harris, K. Butler, J. Shields, S. Kharchenko and J. Douglas, *Polymer*, 2004, **45**, 4227–4239.
17 D. S. Mao, J. H. Chen, L. L. Ren, K. Zhang, M. M. F. Yuen, X. L. Zeng, R. Sun, J. B. Xu and C. P. Wong, *Composites, Part A*, 2019, **123**, 260–269.
18 Z. Y. Zheng, M. Cox and B. Li, *J. Mater. Sci.*, 2018, **53**, 66–99.
19 S. Kong, H. Seo, H. Shin, J.-H. Baik, J. Oh, Y.-O. Kim and J.-C. Lee, *Polymer*, 2019, **180**, 121714.
20 K. Wu, J. M. Wang, D. Y. Liu, C. X. Lei, D. Liu, W. W. Lei and Q. Fu, *Adv. Mater.*, 2020, **32**, 1906939.
21 P. Liu, L. Li, L. Wang, T. Huang, Y. Yao and W. Xu, *J. Alloys Compd.*, 2019, **774**, 396–404.
22 F. Cai, Y. Luo, W. Yang, X. Ye, H. Zhang, J. Zhu and S. Wu, *Mater. Des.*, 2021, **198**, 109335.
23 D. Yang, Y. Ni, X. Kong, D. Gao, Y. Wang, T. Hu and L. Zhang, *Compos. Sci. Technol.*, 2019, **177**, 18–25.
24 V. Guerra, C. Y. Wan and T. McNally, *Prog. Mater. Sci.*, 2019, **100**, 170–186.
25 Y. Jiang, X. Shi, Y. Feng, S. Li, X. Zhou and X. Xie, *Composites, Part A*, 2018, **107**, 657–664.
26 M. Zhu, J. Li, J. Chen, H. Song and H. Zhang, *Comput. Mater. Sci.*, 2019, **164**, 108–115.
27 J. Li, J. Chen, M. Zhu, H. Song and H. Zhang, *Appl. Sci.*, 2019, **9**, 2832.
28 S. Wu, Q. Chen, D. Chen, D. Peng and Y. Ma, *J. Energy Storage*, 2021, **41**, 102931.
29 X. Ma, S. Wu, Z. Yi, D. Peng and J. Zhang, *Int. J. Heat Mass Transfer*, 2019, **137**, 790–798.
30 L. Zhang and L. Liu, *Nanoscale*, 2019, **11**, 3656–3664.
31 J. Li and S. Li, *Mater. Chem. Phys.*, 2021, **274**, 125151.
32 K. Luo, W. Zheng, X. Zhao, X. Wang and S. Wu, *Mater. Des.*, 2018, **154**, 312–325.
33 M. Keshtkar, N. Mehdipour and H. Eslami, *Polymers*, 2019, **11**, 1465.
34 M. Shavikloo and S. Kimiagar, *Comput. Mater. Sci.*, 2017, **139**, 330–334.
35 Y. Wang, C. Yang, Y. Cheng and Y. Zhang, *RSC Adv.*, 2015, **5**, 82638–82644.
36 Y. Li, T. Huang, M. Chen and L. Wu, *Chem. Eng. J.*, 2022, **442**, 136237.
37 B. H. Fan, M. Y. Zhou, C. Zhang, D. L. He and J. B. Bai, *Prog. Polym. Sci.*, 2019, **97**, 101143.
38 L. Y. Wu, K. Wu, D. Y. Liu, R. Huang, J. L. Huo, F. Chen and Q. Fu, *J. Mater. Chem. A*, 2018, **6**, 7573–7584.
39 A. Bashir, M. Maqbool, R. Lv, A. Usman, H. Guo, W. Aftab, H. Niu, M. Liu and S.-L. Bai, *Composites, Part B*, 2021, **218**, 108871.
40 L. Chen, K. Li, B. Li, D. Ren, S. Chen, M. Xu and X. Liu, *Compos. Sci. Technol.*, 2019, **182**, 107741.
41 N. Goldin, H. Dodiuk and D. Lewitus, *Compos. Sci. Technol.*, 2017, **152**, 36–45.
42 Y. Guo, Z. Lyu, X. Yang, Y. Lu, K. Ruan, Y. Wu, J. Kong and J. Gu, *Composites, Part B*, 2019, **164**, 732–739.
43 J.-H. Lee, H. Shin and K. Y. Rhee, *Composites, Part B*, 2019, **157**, 276–282.
44 M. Li, M. Wang, X. Hou, Z. Zhan, H. Wang, H. Fu, C.-T. Lin, L. Fu, N. Jiang and J. Yu, *Composites, Part B*, 2020, **184**, 107746.
45 L. Ren, X. Zeng, R. Sun, J.-B. Xu and C.-P. Wong, *Chem. Eng. J.*, 2019, **370**, 166–175.
46 X. Tian, N. Wu, B. Zhang, Y. Wang, Z. Geng and Y. Li, *Chem. Eng. J.*, 2021, **408**, 127360.
47 Y. Wang, W. Wu, D. Drummer, C. Liu, W. Shen, F. Tomiak, K. Schneider, X. Liu and Q. Chen, *Mater. Des.*, 2020, **191**, 108698.
48 F. Yang, X. Sun, X. Zhang and Z. Yao, *Appl. Surf. Sci.*, 2021, **569**, 151094.
49 Y. Zhan, Z. Long, X. Wan, C. Zhan, J. Zhang and Y. He, *Ceram. Int.*, 2017, **43**, 12109–12119.
50 Y. Zhang, Y. Fan, U. Kamran and S.-J. Park, *Composites, Part A*, 2022, **156**, 106869.
51 Z. Zhang, D. Wu, H. Yang, H. Qu, C. Yao, F. Liu, P. Yu, J. Yao, F. You and X. Jiang, *Chem. Eng. J.*, 2022, **450**, 138247.
52 Z.-B. Zhao, J.-D. Liu, X.-Y. Du, Z.-Y. Wang, C. Zhang and S.-F. Ming, *Colloids Surf., A*, 2022, **635**, 128104.
53 R. Gallu, F. Méchin, F. Dalmas, J.-F. Gérard, R. Perrin and F. Loup, *Constr. Build. Mater.*, 2021, **289**, 123151.
54 Y. L. Luo, R. G. Wang, W. Wang, L. Q. Zhang and S. Z. Wu, *J. Phys. Chem. C*, 2017, **121**, 10163–10173.
55 T. Song, F. Xu, Z. Qin, Y.-T. Pan, Y. Lan, Y. Yang, B. Cheng, D. Li and R. Yang, *Appl. Surf. Sci.*, 2023, **607**, 155100.
56 Y. L. Luo, Y. P. Wu, K. Q. Luo, F. Cai, T. S. Zhai and S. Z. Wu, *Compos. Sci. Technol.*, 2018, **161**, 32–38.
57 H. Yang, F. Cai, Y. Luo, X. Ye, C. Zhang and S. Wu, *Compos. Sci. Technol.*, 2020, **188**, 107971.
58 H. Zhang, F. Cai, Y. Luo, X. Yu and S. Wu, *Polym. Compos.*, 2022, **43**, 5332–5343.
59 L. Zhang and L. J. N. Liu, *Nanoscale*, 2019, **11**, 3656–3664.
60 X.-K. Chen, X.-Y. Hu, P. Jia, Z.-X. Xie and J. Liu, *Int. J. Mech. Sci.*, 2021, **206**, 106576.
61 C. Liu, P. Lu, W. Chen, Y. Zhao and Y. Chen, *Phys. Chem. Chem. Phys.*, 2021, **23**, 26030–26060.
62 K. Fujiwara, M. Daimo, Y. Ueki, T. Ohara and M. Shibahara, *Int. J. Heat Mass Transfer*, 2019, **144**, 118695.